Measuring the Lower Critical Field of Superconductors Using Nitrogen-Vacancy Centers in Diamond Optical Magnetometry

K.R. Joshi, N.M. Nusran, M.A. Tanatar, Kyuil Cho, W.R. Meier, S.L. Bud’ko, P.C. Canfield, and R. Prozorov

Phys. Rev. Applied **11**, 014035 — Published 17 January 2019
DOI: 10.1103/PhysRevApplied.11.014035

Measurements of the lower critical field of superconductors using nitrogen-vacancy centers in diamond optical magnetometry

K. R. Joshi,[1,2] N. M. Nusran,[1,2] M. A. Tanatar,[1,2] Kyuil Cho,[1,2]
W. R. Meier,[1,2] S. L. Bud'ko,[1,2] P. C. Canfield,[1,2] and R. Prozorov[1,2,*]
[1] *Ames Laboratory, Ames, IA 50011*
[2] *Department of Physics & Astronomy, Iowa State University, Ames, IA 50011*
(Dated: 26 June 2018, Revised: 26 December 2018)

The lower critical magnetic field, H_{c1}, of superconductors is measured by optical magnetometry using ensembles of NV-centers-in-diamond. The technique is minimally invasive, allows for accurate detection of the vector magnetic field with sub-Gauss sensitivity and sub-μm spatial resolution. These capabilities are used for detailed characterization of the first vortex penetration into the superconducting samples from the corners. Aided by the revised calculations of the effective demagnetization factors of actual cuboid-shaped samples, these measurements provide precise determination of H_{c1} and related absolute value of London penetration depth, λ. We apply this method to three well-studied superconductors: optimally doped $Ba(Fe_{1-x}Co_x)_2As_2$, stoichiometric $CaKFe_4As_4$, and high-T_c cuprate $YBa_2Cu_3O_{7-\delta}$. Our results are well compared with the values of λ obtained using other techniques, thus adding another non-invasive and sensitive method to measure these important parameters of superconductors.

I. INTRODUCTION

Superconductors remain to be a focus of intense research due to their unusual properties and potential in applications. Cuprates [1] and, more recent, iron based superconductors (IBS) [2] are of particular interest due to their high superconducting transition temperature, T_c, apparently unconventional pairing mechanism [3, 4], and rich interplay of magnetism and superconductivity, including their coexistence in the bulk [5–8].

One of the fundamentally important characteristics of a superconductor is the super-fluid density, which determines the screening of an external magnetic field and is experimentally evaluated from the absolute value of London penetration depth $\lambda(T)$. Accurate measurements of the lower (also known as "first") critical field, H_{c1}, can be used to obtain λ directly, see Eq. 1. These measurements, however, are not simple. The non-spherical shape of the experimental samples leads to distortion of the magnetic fields at sample edges and necessitates vector magnetic field mappings with high spatial resolution of the order of λ, typically in sub-micrometer range. This task was approached by using local probes of magnetic induction, such as miniature Hall probes [9–11], miniature SQUIDs [12] and MFM [13], with spatial resolution in μm range and a sensitivity to a single component of the vector magnetic field.

Among several factors for accurate measurements of H_{c1} three are the most important: (i) The "probe" has to be non-invasive so that local magnetic environment is not disturbed, (ii) it has spatial resolution comparable to λ, and (iii) the demagnetization corrections due to particular sample geometry/shape should be accounted properly, to facilitate proper determination of H_{c1} from measured H_p. Magnetic sensing probes based on Nitrogen-Vacancy (NV) color centers in diamond satisfy the first two requirements. The magnetic moment of the NV-center itself is $\sim \mu_B$ (Bohr magneton), thus minimally perturbs the original magnetic state of the measured specimen. Sub-micrometer spatial resolution can be achieved even with (used here, see experimental section for details) NV ensemble, with probe area of 500 nm diameter and 20 nm thickness [14–18]. Furthermore, the ability to resolve the vector components of the magnetic induction provides a better understanding of how the flux enters the sample.

In this work, we present a novel scheme for accurate measurements of H_{c1} of type-II superconductors using the NV-centers in diamond as an optical probe of local vector magnetic induction. Three different superconductors were measured, including cuprate high$-T_c$, $YBa_2Cu_3O_{7-\delta}$ (YBCO), and IBS, $Ba(Fe_{1-x}Co_x)_2As_2$ and $CaKFe_4As_4$ to demonstrate the performance of this technique. These materials are subject of active current research [19, 20]. For deducing H_{c1}, we used modified demagnetization factors derived for realistic 3D geometries and also compare with outcomes when demagnetization factors calculated from infinite geometries are used [21].

A. Lower critical magnetic field

The lower (first) critical field, H_{c1}, is one of the important fundamental parameters characterizing any type-II superconductor [22]. Above this field, Abrikosov vortices become energetically favorable and start entering the sample from the edges. Importantly, H_{c1} is related to two fundamental length scales: the London penetration depth, λ, and the coherence length ξ, as follows, [23]

* Corresponding author: prozorov@ameslab.gov

$$H_{c1} = \frac{\phi_0}{4\pi\lambda^2}\left(\ln\frac{\lambda}{\xi} + 0.497\right) \quad (1)$$

ξ enters Eq.(1) only under the logarithm and there are other more direct/sensitive ways to determine it experimentally (for example from the upper critical field, $H_{c2} = \phi_0/\left(2\pi\xi^2\right)$, where ϕ_0 =2.07×10^{-15} Wb is magnetic flux quantum. Thus, the London penetration depth λ is often estimated using Eq.(1) if H_{c1} is experimentally given. In terms of the numerical values, for example, for studied here $Ba(Fe_{1-x}Co_x)_2As_2$ (122) iron-based superconductors [5, 24], $\xi \approx 2.3$ nm, $\lambda \approx 200$ nm, so that $\kappa = \lambda/\xi \approx 87$, which give $H_{c1} \approx 200$ Oe and $H_{c2} \approx 60$ T. For optimally - doped YBCO [25–27], $\xi \approx 1.6$ nm, $\lambda \approx 140 - 160$ nm, $\kappa \approx 80 - 100$, $H_{c1} \approx 350 - 400$ Oe and $H_{c2} \approx 120$ T.

In practice, using Eq.(1) to determine H_{c1} has two major difficulties: (1) the existence of various surface barriers [28–30] that inhibit the penetration of a magnetic field, hence lead to over-estimation of H_{c1}, and (2) the distortion of magnetic field around the actual, finite size sample that leads to under-estimation of H_{c1}. Therefore, the experimentally detected onset of the magnetic field penetration, denoted here H_p, coincides with H_{c1} only in case of an infinite slab in a parallel magnetic field and no surface barrier, conditions which are almost impossible to achieve in experiment. However, analysis shows that H_p is directly proportional to H_{c1} with the appropriate geometric conversion factor [30, 31]. Several previous works analyzed the situation and now most experimentalists follow the numerical results published by E. H. Brandt who used approximate nonlinear $E(j)$ characteristics to estimate the connection between H_p and H_{c1} [30, 31]. Here, it is important to understand how H_p is defined.

In Brandt's picture, illustrated in Fig. 1, for samples of a rectangular cross-section $2a\times2c$ (see Fig.2 below), with a magnetic field applied along the $c-$axis, vortices start forming at the corners (where the local field is highest, top right panel of Fig. 1) and propagate as nearly straight segments cutting the corners at approximately 45 degrees (bottom left panel of Fig. 1. When top and bottom segments meet in the middle of the side (at the "equator", bottom right panel of Fig. 1) vortex enters the sample completely. At this value of the applied field, which we denote as H_p^B, the magnetization, $M(H)$, reaches a maximum amplitude and $H_p^B \approx H_{c1}\tanh\sqrt{\alpha c/a}$, where $\alpha = 0.36$ for an infinite (in the $b-$direction) strip or $\alpha = 0.67$ for disks of radius a [30]. Note that at this field a significant volume of the sample is already occupied by vortices (from the corner cutting) and a local magnetic field at the corners has far exceeded H_{c1}.

An alternative definition of H_p is based on the deviation of local magnetic induction from zero or total magnetic moment from linear $M(H)$ behavior. In practice, the local magnetic induction, B, is measured outside the sample, on its surface close to the sample edge. The external magnetic field expelled by the sample leaks into

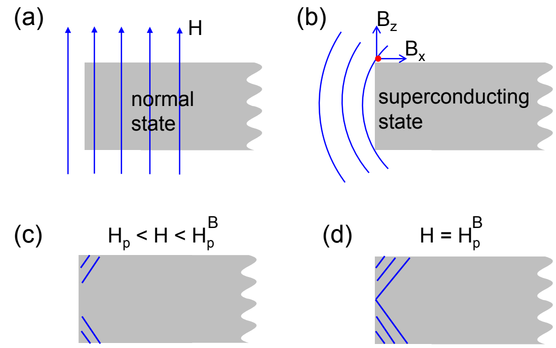

FIG. 1. (a) Schematics of applied magnetic field fully penetrating the superconductor at its normal state, (b) total expulsion of the magnetic flux at its superconducting state, (c) magnetic field entering from the corners of the sample with an angle approximately 45^0 , and (d) E. H. Brandts' scenario when applied magnetic field is equal to H_p^B. (See text for details.)

the sensor, so that measured $B(H)$ is always non zero, but is still linear in H and it deviates from linearity when vortices start to penetrate the sample from the corners and this can be detected as the the onset of flux penetration field H_p [11, 32]. Similar estimate can be obtained from the $M(H)$ curves detecting the deviation from linear behavior upon application of a magnetic field after cooling in zero field [33]. Another version of this approach is to look for the remnant flux trapped inside the superconductor which becomes non-zero when a lower critical field is reached in any part of the sample, vortices penetrated and became trapped due to ubiquitous pinnings [34]. In all these scenarios, the lower critical field should be obtained with the appropriate effective demagnetization factor, N,

$$H_p = H_{c1}\left(1 + N\chi\right) \quad (2)$$

where χ is the "intrinsic" magnetic susceptibility of the material (i.e., in an "ideal" sample with no demagnetization and surface barriers), which can be taken to be equal to -1 for a robust superconductor at most temperatures below T_c (for an infinite slab of width $2w$ in a parallel field, $\chi = \lambda/w\tanh\left(w/\lambda\right) - 1$ and it is straightforward to check that χ is still less than -0.995 even at $T/T_c = 0.99$).

Unfortunately, most previous works that employed local measurements of the onset of magnetic flux penetration using, for example, miniature Hall probes [11, 32, 34], analyzed the data with Brandt's formulas for H_p^B and not with the (more correct in this case) H_p from Eq.(2).

B. Effective demagnetizing factors

To use H_p for determining H_{c1}, the effective demagnetizing factor, N, has to be calculated for specific sample geometry. Indeed, strictly speaking, N is only defined for ellipsoidal samples, which is of little practical use for typical samples of a cuboidal (rectangular plate) shape. Yet, it is possible to introduce effective demagnetizing factors which were calculated in several previous works, including the cited Brandt's papers, since his estimate of H_p^B implicitly includes the effective N [31]. As we recently showed from a full 3D finite-element analysis [21], Brandt provided very accurate expressions for demagnetizing factors in cases of infinite strips or disks of rectangular cross-section, see Eq.(7) in Ref.[31]. However, we also found that the effective demagnetizing factors for finite cuboids are quite different from the infinite 2D strips and, therefore, the whole methodology of estimating H_{c1} from magnetic measurements should be revisited. This is the subject of the present work.

Although we can calculate the effective demagnetization factor with arbitrary precision for a sample of any shape, it is always useful to have simple, but accurate enough formulas [21]. A good approximation for a $2a \times 2b \times 2c$ cuboid in a magnetic field along the $c-$direction is given by [21],

$$N^{-1} = 1 + \frac{3}{4}\frac{c}{a}\left(1 + \frac{a}{b}\right) \tag{3}$$

Having samples of rectangular cross-section is problematic from the uncertainty in demagnetization effects point of view, but it is advantageous in terms of the (absence) of surface barriers, because now magnetic flux penetrates from the corners and not parallel to the extended flat surfaces which is how surface barriers are formed [28]. Moreover, the "geometric barrier" that essentially involves the flux corner penetration described above [30, 31] is not relevant if the onset of nonlinearity is detected near the sample edge.

II. EXPERIMENTAL

A. Optical magnetic sensing using NV centers in diamond

In this work, the vector magnetic induction on the sample surface was measured using optical magnetometry based on nitrogen-vacancy (NV) color centers in diamond. Specifically, the optically detected magnetic resonance (ODMR) of Zeeman split energy levels in NV centers, proportional to a local magnetic field, is measured [35]. The NV-centers' magneto-sensing has several important advantages for measurements of delicate effects in superconductors. (1) It is minimally invasive, - the magnetic moment of the probe itself is of the order of a few Bohr magnetons, μ_B, and hence has negligible effect on the measured magnetic fields. (2) It has sufficient spatial resolution, - sub-micrometer spatial mapping can be achieved even with the ensemble mode of NV sensing. (3) It is capable to measure a vector magnetic induction [36]. This is particularly important as the detection of flux penetration depends on the location, and magnetic field lines deviate significantly from the direction of the applied field [21].

Measurement protocols, experimental schematics and deconvolution of the ODMR spectrum into magnetic field components are discussed in detail in our previous work in which the spatial structure of the Meissner state in various superconductors was studied [36]. Here, we focus particularly on the measurements of the lower critical field, H_{c1}, and summarize the key experimental details for completeness.

To measure a local magnetic induction, a magneto-optical "indicator" ($1.5 \times 1 \times 0.04$ mm^3 diamond plate with embedded NV centers) is placed on top of the superconducting sample with its NV-active side facing the sample surface. On the "active" side, NV centers are created within ~ 20 nm from the surface of a single crystalline diamond plate using commercial protocols that involve nitrogen ion implantation, electron irradiation and high temperature annealing in high vacuum. The diamond plate has (100) crystal surface and [100] edges. Therefore, NV centers are oriented along all four [111] diamond axes, which define the directions of the magnetic field sensing. As a result, possible Zeeman splittings in a random ensemble of NV centers in (indeed, a single crystal of) diamond is given by $2\gamma_e|\vec{B} \cdot \hat{d}|$, where $\gamma_e \approx 2.8$ MHz/G is the gyromagnetic ratio of the NV-center electronic spin, and $\hat{d}$ is a unit vector along any of the four diamond axes. In a magnetic field along the $\hat{z}$ direction, i.e., $\vec{B} = (0, 0, B_z)$, all possible NV orientations result in the same splitting,

$$Z = \frac{2\gamma_e B_z}{\sqrt{3}} \approx 3.233 \text{ MHz/G}$$

whereas, if the magnetic field has two components such that $\vec{B} = (B_x, 0, B_z)$, the NV ensemble will result in two pairs of Zeeman splittings:

$$Z_{L,S} = Z|B_z \pm B_x|$$

where, Z_L (Z_S) refers to larger (smaller) Zeeman splitting. An example of such two-pairs of ODMR splitting spectrum is shown in Fig.2(b).

B. Experimental

Experimental setup: The experimental setup is based on the Attocube CFM/AFM system and includes a confocal microscope optimized for the NV fluorescence detection inside the helium cryostat with optical parts in vacuum and the sample placed on a temperature-controlled cold stage. A schematic of the experiment is shown in Fig.2(a). The objective is focused on the NV centers in a

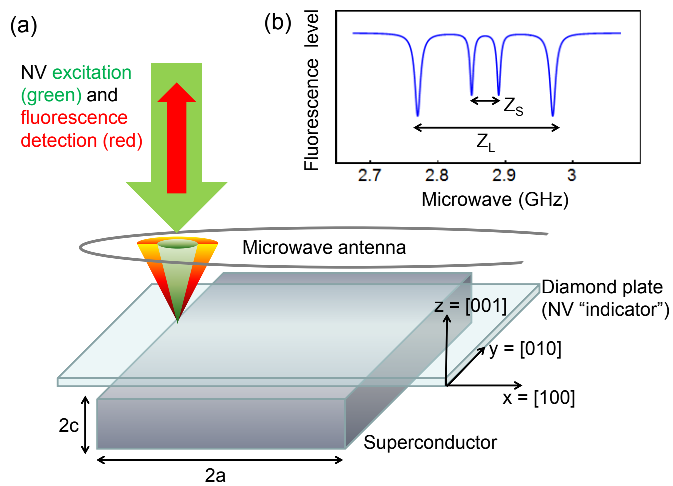

FIG. 2. (Color online)(a) Schematics of the key components of the NV sensing setup (b) Optically detected magnetic resonance (ODMR) spectrum for local magnetic field vector with two components, $\vec{B} = (B_x, 0, B_z)$. (See text for details.)

(optically transparent) diamond plate, so that the convolution of the diffraction limited confocal volume with the NV distribution leads to essentially a disk shaped sensing volume of thickness $\approx$ 20 nm and diameter $\approx$ 500 nm. The diamond plate is placed directly on top of a flat sample surface covering the edge and with NV active side facing the sample. More importantly, the superconducting sample edges are carefully aligned with diamond edges so that when the superconductor is in the Meissner state, the vector magnetic field at the probing point will have no component along [010] diamond crystal direction. This symmetry of placement guarantees only two pairs of Zeeman splitting in the ODMR. A 50X confocal microscope objective is used both for green laser excitation and red fluorescence collection. Microwave radiation with a very small amplitude is applied using a single-turn 50 μm diameter silver wire.

Temperature variation during measurements: The laser and microwave power used in these experiments are approximately 500 μW and less than 0 dBm, respectively. While no noticeable effect was observed due to the laser, microwave excitation showed some small change in the base temperature fluctuating between 4.2 and 4.3 K. Therefore, all our experiments were performed at 4.5 K with active temperature control keeping the stability within 10 mK. These fluctuations are much lower than reported previously in Ref.[37], probably because our microwave loop antenna geometry is more optimized for the experiment.

Spatial resolution: Spatial resolution of the probe here is governed by the optical diffraction limit, resulting $\approx$500 nm lateral resolution. One possibility of improving the lateral resolution is to incorporate super-resolution imaging techniques [38, 39]. Another possibility is to use nanoscale scanning NV probes [40–42]. In fact, magnetic imaging of individual Abrikosov vorteces were already demonstrated using scanning single NV probes in Refs.[43, 44]. The imaged superconducting materials in these works were field-cooled to the superconducting state in the presence of a weak external background magnetic field in order to form a well isolated vortex distribution.

Integration time: In our H_{c1} measurements, for each data point (a given position and external magnetic field), ODMR spectrum was obtained for a 50-100 MHz scan range averaged for ten repetitions. The typical total integration time per data point is 5-10 minutes. In order to speed up the experiments, one could use adaptive protocols to modify/optimize scan range and number of averages according to the previous measurement outcomes. Another possibility is to incorporate real-time lock-in detection techniques [45].

Samples: All samples were pre-characterized using various thermodynamic and transport techniques (see, e.g., Ref. [46]) and imaged using scanning electron microscopy (SEM) and only samples with well-defined surfaces and edges, as shown in Fig.3(a), were selected for further measurements.

III. MEASUREMENTS OF THE LOWER CRITICAL FIELD

The experimental protocol for measurements of H_{c1} is as follows:

(1) The sample is cooled to the target temperature below T_c in the absence of a magnetic field (zero-field cooling, ZFC). Then, a small magnetic field (10 Oe in our case, much smaller than 200 - 400 Oe expected for H_{c1} at low temperatures as discussed in the introduction) is applied and ODMR signals are recorded at different points along the line perpendicular to the sample edge. Measured ODMR splittings are then converted into the magnetic induction values as described above. This, combined with direct visualization of the sample through a transparent diamond plate, allows for accurate determination of the location of the sample edge and provides information about sample homogeneity. The quality of the superconductor is also verified by looking at the sharpness of the transition detected by the ODMR splitting recorded as a function of temperature at any fixed point over the sample, see, e.g., Fig.3(b).

(2) After this initial preparation and edge identification, the magnetic field is removed, the sample is warmed up to above T_c and then cooled back down to a target temperature, thereby resetting it to the genuine superconducting state with no trapped magnetic field inside. A point inside and over the sample, but close to the edge, is chosen and ODMR spectra are recorded as a function of external magnetic field, which is applied incrementally in small steps. At each step, the superconducting magnet is switched to a persistent mode to insure stability of the magnetic field. The deviation from the linear behavior

in Z_S is then detected and recorded as the field of first flux penetration, H_p.

(3) Now, using Eq.(2), (3), and (1), the value of H_{c1} and the London penetration depth λ are evaluated. This procedure is repeated at several locations along the edge to ensure objectivity of the result.

IV. RESULTS AND DISCUSSION

To illustrate the described method, we measured H_{c1} and evaluated the London penetration depth, λ, in three different superconducting materials.

A. $\mathbf{Ba(Fe_{1-x}Co_x)_2As_2}$, $x = 0.07$

A well characterized optimally doped single crystal of $Ba(Fe_{1-x}Co_x)_2As_2$, $x = 0.07$ (FeCo122) of cuboidal shape with dimensions, $1.0{\times}1.2{\times}0.05$ mm^3, was selected. An SEM image in Fig.3(a) shows a well-defined prismatic corner with flat clean surface and straight edges. The superconducting transition temperature, $T_c \approx 24$ K, determined from a conventional magnetometer, was also consistent with our ODMR measurements at the location on the sample surface inside the sample as shown in Fig.3(b). ODMR splittings at four different locations on the sample surface near the edge are labeled A, B, C, and D in Fig.3(c). These four points are approximately 5 μm far apart from neighbor points and each point is approximately 10 μm from the edge inside the sample. As discussed above, the two Zeeman splittings Z_L and Z_S correspond to linear combinations of horizontal (B_x) and vertical (B_z) components of the magnetic induction as described above. Notice excellent reproducibility of the results indicating homogeneous superconducting properties of our sample. The inset Fig.3(c) shows average (of four points) small splitting signal (Z_S). A clear onset of first flux penetration is determined at at H_p=13.2±1 Oe.

To understand the observed ODMR splittings, we consider Brandt's results of flux corner cutting and entering in form of Abrikosov vortices approximately at an angle of 45^0 with respect to the corner. Therefore the normal to the sample surface z-component (along the applied field) and longitudinal, x-component of the magnetic induction are approximately equal and proportional to the applied field. This linear relation continues with the increasing applied field until a critical value of the first flux penetration field, H_p, is reached. At this point, angle of the magnetic flux at the sample edges deviates from 45^0 trending more towards $\hat{z}$ direction. This scenario can be phenomenologically modeled by representing the magnetic induction components as: $B_{z,x} = DH \pm \delta$ and $\delta = 0 + \alpha\theta(H - H_p)(H - H_p)^n$ where D is an effective demagnetization factor and $\theta(H)$ is a Heaviside step function. Because the larger splitting -Z_L and smaller splitting -Z_S are proportional to the sum and difference of $B_{z,x}$ components respectively, the change at H_p is reflected clearly in Z_S but not in Z_L. The Zeeman splittings observed in Fig.3(c) can be understood with this model for the parameters: $D = 3.5$, $H_p = 13.2$, $\alpha = 0.6$, and $n = 1$. Hence, this provides an experimental confirmation for Brandt's description of flux corner cutting and entering approximately at an angle of 45^0 with respect to its sides.

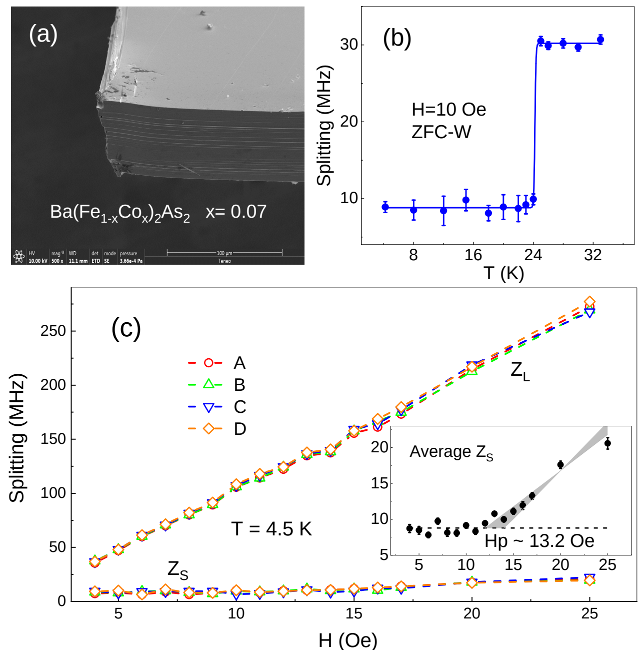

FIG. 3. (Color online)(a) Scanning electron microscope (SEM) image of the measured single crystal of $Ba(Fe_{1-x}Co_x)_2As_2$, x=0.07 (b) Detection of superconducting phase transition at $T_c \approx 24$ K. Each data point in the plot was obtained from 4 minutes total integration time of the ODMR. Error bars represent the standard errors extracted from the double Lorentz function fitting parameters for the dip position (not shown here). (c) H_{c1} measurements of this sample at 4.5 K. Zeeman splittings measured at four different points, A, B, C and D near the edge as a function of the increasing magnetic field applied after ZFC. The 4-point-averaged signal of the Z_S is shown in the inset; a clear "change" at H_p=13.2±1 Oe is observed. Shaded area visually captures the spread of measurements after this change - from which the error of H_p is determined.

From the experimental value of H_p and effective demagnetization factor for this particular sample, $N = 0.9168$ we obtain using Eq.(2), H_{c1} =158±12 Oe. And with the use of Eq.(1) and taking $\xi \approx 2.3$ nm, we obtain the final result, $\lambda = 226{\pm}10$ nm. This estimate for penetration depth is comparable with the values obtained from other techniques such as μSR - 224 nm [47] and MFM - 245 nm [48]. The agreement is quite remarkable and gives confidence in the validity of the developed technique. Table (I) summarize all these estimates. Estimates obtained using Brandt's formulas are also given for comparison.

Superconductor	T_c (K)	H_{c1}^{2D} (G)	λ_{ab}^{2D} (nm)	H_{c1} (G)	λ_{ab} (nm)	λ (nm) from literature
FeCo122	24.3	102±8	288±12	158±12	226±10	270,245,224 [47–49]
$CaKFe_4As_4$	34	139±18	251±18	394±52	141±11	208,187 [50]
YBCO	88.3	163±15	236±12	344±31	156±8	146,160,155,149 [26, 51–53]

TABLE I. Estimates forH_{c1} and λ_{ab}. Here "2D" refers to values obtained using Barndt's formulas.

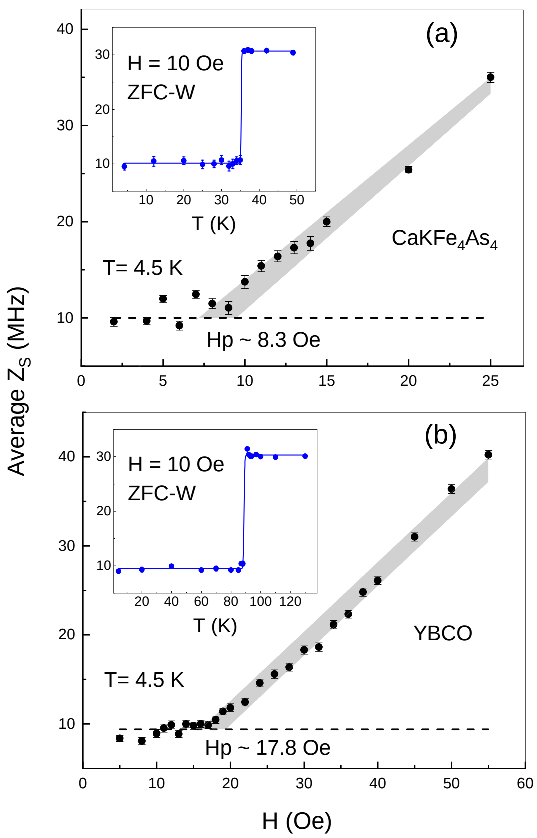

FIG. 4. Measurements of the field of first flux penetration, H_p, in single crystals of (a) $CaKFe_4As_4$ and (b) $YBa_2Cu_3O_{7-\delta}$. Insets show superconducting phase transitions at $T_c \approx 34$ K and 88 K, respectively.

B. $CaKFe_4As_4$

The cuboid - shaped single crystal of stoichiometric $CaKFe_4As_4$ with dimensions of $1.01 \times 0.99 \times 0.01$ mm^3 was studied. The inset in Fig.4(a) shows a sharp superconducting phase transition at $T_c \approx 34$ K. The average of ODMR splitting, Z_S, near the sample edge as a function of the applied magnetic field clearly shows a break associated with the magnetic flux penetration at $H_p = 8.3 \pm 1.1$ Oe. The error here is determined visually by the shaded region which spans all measurement points. Using Eq.(2) and (3), this results in the estimation of $H_{c1} = 394 \pm 52$ Oe. Now, using Eq.(1) and $\xi \approx 2.15$ nm [46], we estimate $\lambda = 141 \pm 11$ nm. This result was used to calculate the superfluid density in Ref.[46], which was consistent with isotropic two-gap $s_\pm$ pairing state.

C. $YBa_2Cu_3O_{7-\delta}$

To look at a very different system, we also measured a single crystal of a well known cuprate superconductor, $YBa_2Cu_3O_{7-\delta}$ (YBCO). The sample dimensions were $0.5 \times 0.85 \times 0.017$ mm^3. The inset in Fig.4(b) shows a sharp superconducting phase transition at $T_c \approx 88$ K. The clear break associated with the magnetic field of first flux penetration in the average Z_S vs H plot is observed at H_p=17.8±1.6 Oe. Using Eq.(2) and (3), this leads to estimation of $H_{c1} = 344 \pm 31$ Oe. Using Eq.(1) and coherence length $\xi \approx 1.6$ nm [25, 27], we estimate $\lambda \approx 156 \pm 8$ nm. All estimates including values obtained using Barndt's formulas and from other techniques are summarized in Table (I). Once again a good agreement is seen between our estimates and the values reported in the literature obtained from other techniques such as μSR - 155 nm [52], microwave cavity perturbation technique, 160 nm [51] and tunnel-diode resonator, 140 nm [26].

V. CONCLUSIONS

In summary we used NV-centers in diamond for optical vector magnetic field sensing at low temperatures to measure the lower critical field, H_{c1}, in type II superconductors. The minimally-invasive nature and optical diffraction-limited small size of the probe makes NV sensor ideal for this purpose. The capability of resolving vector components provides a unique advantage, which allowed direct verification of the E. H. Brandt's model of magnetic flux penetration that proceeds via corner cutting by vortices at $\approx 45^0$ angle with respect to the edges. We applied this technique to three different superconductors: optimally doped FeCo122, stoichiometric $CaKFe_4As_4$, and high-T_c cuprate, YBCO. London penetration depth values evaluated from the obtained H_{c1} are in a good agreement with the literature with the largest uncertainty for CaK1144, most likely due to various levels of scattering in samples studied in different works. Our approach is very useful non-invasive way to estimate $\lambda(0)$ that is needed to obtain superfluid density, which is the quantity that can be compared with theory.

ACKNOWLEDGEMENT

This work was supported by the U.S. Department of Energy (DOE), Office of Science, Basic Energy Sciences, Materials Science and Engineering Division. The research was performed at Ames Laboratory, which is operated for the U.S. DOE by Iowa State University under contract # DE-AC02-07CH11358. W. M. was supported by the Gordon and Betty Moore Foundation's EPiQS Initiative through Grant GBMF4411.

---

[1] J.G. Bednorz and K.A. Müller, "Possible high T_c superconductivity in the Ba-La-Cu-O system," Z. Phys. B **64**, 189 (1986).

[2] Yoichi Kamihara, Takumi Watanabe, Masahiro Hirano, and Hideo Hosono, "Iron-Based Layered Superconductor $La[O_{1-x}F_x]FeAs$ (x = 0.05−0.12) with $T_c = 26$ K," J. Am. Chem. Soc. **130**, 3296 (2008).

[3] C. C. Tsuei and J. R. Kirtley, "Pairing symmetry in cuprate superconductors," Rev. Mod. Phys. **72**, 969 (2000).

[4] I.I. Mazin, "Superconductivity gets an iron boost," Nature **464**, 183 (2010).

[5] Paul C. Canfield and Sergey L. Bud'ko, "FeAs-Based Superconductivity: A Case Study of the Effects of Transition Metal Doping on $BaFe_2As_2$," Annu. Rev. Condens. Matter Phys. **1**, 27 (2010).

[6] David C. Johnston, "The puzzle of high temperature superconductivity in layered iron pnictides and chalcogenides," Adv. Phys. **59**, 803 (2010).

[7] G. R. Stewart, "Superconductivity in iron compounds," Rev. Mod. Phys. **83**, 1589 (2011).

[8] R.M. Fernandes, A.V. Chubukov, and J. Schmalian, "What drives nematic order in iron-based superconductors?" Nat. Phys. **10**, 97 (2014).

[9] M Konczykowski, F Holtzberg, and P Lejay, "Local Hall probe magnetometry: a new technique for investigation of magnetic flux penetration, exclusion and trapping in HTSC," Supercond. Sci. Technol. **4**, S331 (1991).

[10] C. Putzke, P. Walmsley, J. D. Fletcher, L. Malone, D. Vignolles, C. Proust, S. Badoux, P. See, H. E. Beere, D. A. Ritchie, S. Kasahara, Y. Mizukami, T. Shibauchi, Y. Matsuda, and A. Carrington, "Anomalous critical fields in quantum critical superconductors," Nat. Commun. **5**, 5679 (2014).

[11] T. Klein, D. Braithwaite, A. Demuer, W. Knafo, G. Lapertot, C. Marcenat, P. Rodière, I. Sheikin, P. Strobel, A. Sulpice, and P. Toulemonde, "Thermodynamic phase diagram of $Fe(Se_{0.5}Te_{0.5})$ single crystals in fields up to 28 tesla," Phys. Rev. B **82**, 184506 (2010).

[12] Clifford W. Hicks, Thomas M. Lippman, Martin E. Huber, James G. Analytis, Jiun-Haw Chu, Ann S. Erickson, Ian R. Fisher, and Kathryn A. Moler, "Evidence for a Nodal Energy Gap in the Iron-Pnictide Superconductor LaFePO from Penetration Depth Measurements by Scanning SQUID Susceptometry," Phys. Rev. Lett. **103**, 127003 (2009).

[13] Lan Luan, Ophir M. Auslaender, Thomas M. Lippman, Clifford W. Hicks, Beena Kalisky, Jiun-Haw Chu, James G. Analytis, Ian R. Fisher, John R. Kirtley, and Kathryn A. Moler, "Local measurement of the penetration depth in the pnictide superconductor $Ba(Fe_{0.95}Co_{0.05})_2As_2$," Phys. Rev. B **81**, 100501 (2010).

[14] Francesco Casola, Toeno van der Sar, and Amir Yacoby, "Probing condensed matter physics with magnetometry based on nitrogen-vacancy centres in diamond," Nat. Rev. Mater. **3**, 17088 (2018).

[15] J.-P. Tetienne, N. Dontschuk, D.A. Broadway, A. Stacey, D.A. Simpson, and L.C.L. Hollenberg, "Quantum imaging of current flow in graphene," Sci. Adv. **3**, e1602429 (2017).

[16] L. Rondin, J.-P. Tetienne, T. Hingant, J.-F. Roch, P. Maletinsky, and V. Jacques, "Magnetometry with nitrogen-vacancy defects in diamond," Rep. Prog. Phys. **77**, 056503 (2014).

[17] Romana Schirhagl, Kevin Chang, Michael Loretz, and Christian L. Degen, "Nitrogen-vacancy centers in diamond: Nanoscale Sensors for Physics and Biology," Annu. Rev. Phys. Chem. **65**, 83 (2014).

[18] L. M. Pham, D. Le Sage, P. L. Stanwix, T. K. Yeung, D. Glenn, A. Trifonov, P. Cappellaro, P. R. Hemmer, M. D. Lukin, H. Park, A. Yacoby, and R. L. Walsworth, "Magnetic field imaging with nitrogen-vacancy ensembles," New J. Phys. **13**, 045021 (2011).

[19] Akira Iyo, Kenji Kawashima, Tatsuya Kinjo, Taichiro Nishio, Shigeyuki Ishida, Hiroshi Fujihisa, Yoshito Gotoh, Kunihiro Kihou, Hiroshi Eisaki, and Yoshiyuki Yoshida, "New-Structure-Type Fe-Based Superconductors: $CaAFe_4As_4$ (A = K, Rb, Cs) and $SrAFe_4As_4$ (A = Rb, Cs)," J. Am. Chem. Soc. **138**, 3410 (2016).

[20] W. R. Meier, T. Kong, U. S. Kaluarachchi, V. Taufour, N. H. Jo, G. Drachuck, A. E. Böhmer, S. M. Saunders, A. Sapkota, A. Kreyssig, M. A. Tanatar, R. Prozorov, A. I. Goldman, Fedor F. Balakirev, Alex Gurevich, S. L. Bud'ko, and P. C. Canfield, "Anisotropic thermodynamic and transport properties of single-crystalline $CaKFe_4As_4$," Phys. Rev. B **94**, 064501 (2016).

[21] R. Prozorov and V. G. Kogan, "Effective Demagnetizing Factors of Diamagnetic Samples of Various Shapes," Phys. Rev. Applied **10**, 014030 (2018).

[22] M. Tinkham, *Introduction to Superconductivity*, 2nd ed., Dover Books on Physics (Dover Publications, 2004).

[23] Chia-Ren Hu, "Numerical Constants for Isolated Vortices in Superconductors," Phys. Rev. B **6**, 1756 (1972).

[24] R. Prozorov and V. G. Kogan, "London penetration depth in iron-based superconductors," Rep. Prog. Phys. **74**, 124505 (2011).

[25] K. E. Gray, D. H. Kim, B. W. Veal, G. T. Seidler, T. F. Rosenbaum, and D. E. Farrell, "High anisotropy and a dimensionality crossover in the irreversibility behavior of oxygen-deficient $YBa_2Cu_3O_{7-y}$," Phys. Rev. B **45**, 10071 (1992).

[26] R. Prozorov, R. W. Giannetta, A. Carrington, P. Fournier, R. L. Greene, P. Guptasarma, D. G. Hinks, and A. R. Banks, "Measurements of the absolute value of the penetration depth in high-T_c superconductors using a low-T_c superconductive coating," Appl. Phys. Lett. **77**, 4202 (2000).

[27] T. Sekitani, N. Miura, S. Ikeda, Y. H. Matsuda, and Y. Shiohara, "Upper critical field for optimally-doped $YBa_2Cu_3O_{7-\delta}$," Physica B: Condensed Matter **346-347**, 319 (2004).

[28] C. P. Bean and J. D. Livingston, "Surface Barrier in Type-II Superconductors," Phys. Rev. Lett. **12**, 14 (1964).

[29] E H Brandt, "The flux-line lattice in superconductors," Rep. Prog. Phys. **58**, 1465 (1995).

[30] Ernst Helmut Brandt, "Geometric barrier and current string in type-II superconductors obtained from continuum electrodynamics," Phys. Rev. B **59**, 3369 (1999).

[31] E. H. Brandt, "Geometric edge barrier in the Shubnikov phase of type-II superconductors," Low Temp. Phys. **27**, 723 (2001).

[32] R. Okazaki, M. Konczykowski, C. J. van der Beek, T. Kato, K. Hashimoto, M. Shimozawa, H. Shishido, M. Yamashita, M. Ishikado, H. Kito, A. Iyo, H. Eisaki, S. Shamoto, T. Shibauchi, and Y. Matsuda, "Lower critical fields of superconducting $PrFeAsO_{1-y}$ single crystals," Phys. Rev. B **79**, 064520 (2009).

[33] M. Abdel-Hafiez, J. Ge, A. N. Vasiliev, D. A. Chareev, J. Van de Vondel, V. V. Moshchalkov, and A. V. Silhanek, "Temperature dependence of lower critical field $H_{c1}(T)$ shows nodeless superconductivity in FeSe," Phys. Rev. B **88**, 174512 (2013).

[34] Z. Pribulova, T. Klein, J. Kacmarcik, C. Marcenat, M. Konczykowski, S. L. Bud'ko, M. Tillman, and P. C. Canfield, "Upper and lower critical magnetic fields of superconducting $NdFeAsO_{1-x}F_x$ single crystals studied by Hall-probe magnetization and specific heat," Phys. Rev. B **79**, 020508 (2009).

[35] L. Rondin, J. P. Tetienne, S. Rohart, A. Thiaville, T. Hingant, P. Spinicelli, J. F. Roch, and V. Jacques, "Stray-field imaging of magnetic vortices with a single diamond spin," Nat. Commun. **4**, 2279 (2013).

[36] N M Nusran, K R Joshi, K Cho, M A Tanatar, W R Meier, S L Budko, P C Canfield, Y Liu, T A Lograsso, and R Prozorov, "Spatially-resolved study of the meissner effect in superconductors using NV-centers-in-diamond optical magnetometry," New J. Phys. **20**, 043010 (2018).

[37] Dominik Rohner, Lucas Thiel, Benedikt Müller, Mark Kasperczyk, Reinhold Kleiner, Dieter Koelle, and Patrick Maletinsky, "Real-space probing of the local magnetic response of thin-film superconductors using single spin magnetometry," Sensors **18**, 3790 (2018).

[38] Eva Rittweger, Kyu Young Han, Scott E. Irvine, Christian Eggeling, and Stefan W. Hell, "STED microscopy reveals crystal colour centres with nanometric resolution," Nature Photon. **3**, 144 (2009).

[39] Edward H. Chen, Ophir Gaathon, Matthew E. Trusheim, and Dirk Englund, "Wide-Field Multispectral Super-Resolution Imaging Using Spin-Dependent Fluorescence in Nanodiamonds," Nano Lett. **13**, 2073 (2013).

[40] P. Maletinsky, S. Hong, M.S. Grinolds, B. Hausmann, M.D. Lukin, R.L. Walsworth, M. Loncar, and A. Yacoby, "A robust scanning diamond sensor for nanoscale imaging with single nitrogen-vacancy centres," Nat. Nanotechnol. **7**, 320 (2012).

[41] Patrick Appel, Elke Neu, Marc Ganzhorn, Arne Barfuss, Marietta Batzer, Micha Gratz, Andreas Tschoepe, and Patrick Maletinsky, "Fabrication of all diamond scanning probes for nanoscale magnetometry," Rev. Sci. Instrum. **87**, 063703 (2016).

[42] Tony X. Zhou, Rainer J. Stoehr, and Amir Yacoby, "Scanning diamond NV center probes compatible with conventional AFM technology," Appl. Phys. Lett. **111**, 163106 (2017).

[43] L. Thiel, D. Rohner, M. Ganzhorn, P. Appel, E. Neu, B. Mller, R. Kleiner, D. Koelle, and P. Maletinsky, "Quantitative nanoscale vortex imaging using a cryogenic quantum magnetometer," Nat. Nanotechnol. **11**, 677 (2016).

[44] M. Pelliccione, A. Jenkins, P. Ovartchaiyapong, C. Reetz, E. Emmanouilidou, N. Ni, and A.C. Bleszynski Jayich, "Scanned probe imaging of nanoscale magnetism at cryogenic temperatures with a single-spin quantum sensor," Nat. Nanotechnol. **11**, 700 (2016).

[45] Rolf Simon Schoenfeld and Wolfgang Harneit, "Real Time Magnetic Field Sensing and Imaging Using a Single Spin in Diamond," Phys. Rev. Lett. **106**, 030802 (2011).

[46] Kyuil Cho, A. Fente, S. Teknowijoyo, M. A. Tanatar, K. R. Joshi, N. M. Nusran, T. Kong, W. R. Meier, U. Kaluarachchi, I. Guillamón, H. Suderow, S. L. Bud'ko, P. C. Canfield, and R. Prozorov, "Nodeless multiband superconductivity in stoichiometric single-crystalline $CaKFe_4As_4$," Phys. Rev. B **95**, 100502 (2017).

[47] T. J. Williams, A. A. Aczel, E. Baggio-Saitovitch, S. L. Bud'ko, P. C. Canfield, J. P. Carlo, T. Goko, H. Kageyama, A. Kitada, J. Munevar, N. Ni, S. R. Saha, K. Kirschenbaum, J. Paglione, D. R. Sanchez-Candela, Y. J. Uemura, and G. M. Luke, "Superfluid density and field-induced magnetism in $Ba(Fe_{1-x}Co_x)_2As_2$ and $Sr(Fe_{1-x}Co_x)_2As_2$ measured with muon spin relaxation," Phys. Rev. B **82**, 094512 (2010).

[48] Lan Luan, Thomas M. Lippman, Clifford W. Hicks, Julie A. Bert, Ophir M. Auslaender, Jiun-Haw Chu, James G. Analytis, Ian R. Fisher, and Kathryn A. Moler, "Local Measurement of the Superfluid Density in the Pnictide Superconductor $Ba(Fe_{1-x}Co_x)_2As_2$ across the Superconducting Dome," Phys. Rev. Lett. **106**, 067001 (2011).

[49] R. T. Gordon, H. Kim, N. Salovich, R. W. Giannetta, R. M. Fernandes, V. G. Kogan, T. Prozorov, S. L. Bud'ko, P. C. Canfield, M. A. Tanatar, and R. Prozorov, "Doping evolution of the absolute value of the london penetration depth and superfluid density in single crystals of $Ba(Fe_{1-x}Co_x)_2As_2$," Phys. Rev. B **82**, 054507 (2010).

[50] Rustem Khasanov, William R. Meier, Yun Wu, Daixiang Mou, Sergey L. Bud'ko, Ilya Eremin, Hubertus Luetkens, Adam Kaminski, Paul C. Canfield, and Alex Amato, "In-plane magnetic penetration depth of superconducting $CaKFe_4As_4$," Phys. Rev. B **97**, 140503 (2018).

[51] Dong-Ho Wu, W. L. Kennedy, C. Zahopoulos, and S. Sridhar, "Characteristics and growth of single crystals of $Y_1Ba_2Cu_3O_7$ with superior microwave properties," Appl. Phys. Lett. **55**, 696 (1989).

[52] J. L. Tallon, C. Bernhard, U. Binninger, A. Hofer, G. V. M. Williams, E. J. Ansaldo, J. I. Budnick, and Ch. Niedermayer, "In-Plane Anisotropy of the Penetration Depth Due to Superconductivity on the Cu-O Chains in $YBa_2Cu_3O_{7-\delta}$,$Y_2Ba_4Cu_7O_{15-\delta}$, and $YBa_2Cu_4O_8$," Phys. Rev. Lett. **74**, 1008 (1995).

[53] J. E. Sonier, R. F. Kiefl, J. H. Brewer, D. A. Bonn, J. F. Carolan, K. H. Chow, P. Dosanjh, W. N. Hardy, Ruixing Liang, W. A. MacFarlane, P. Mendels, G. D. Morris,

T. M. Riseman, and J. W. Schneider, "New muon-spin-rotation measurement of the temperature dependence of the magnetic penetration depth in $YBa_2Cu_3O_{6.95}$," Phys. Rev. Lett. **72**, 744 (1994).